nature communications

Article

https://doi.org/10.1038/s41467-024-51194-z

Optoelectronic synapses with chemical-electric behaviors in gallium nitride semiconductors for biorealistic neuromorphic functionality

Received: 29 January 2024

Accepted: 30 July 2024

Published online: 03 September 2024

Check for updates

A list of authors and their affiliations appears at the end of the paper

Optoelectronic synapses, leveraging the integration of classic photo-electric effect with synaptic plasticity, are emerging as building blocks for artificial vision and photonic neuromorphic computing. However, the fundamental working principles of most optoelectronic synapses mainly rely on physical behaviors while missing chemical-electric synaptic processes critical for mimicking biorealistic neuromorphic functionality. Herein, we report a photoelectrochemical synaptic device based on p-AlGaN/n-GaN semiconductor nanowires to incorporate chemical-electric synaptic behaviors into optoelectronic synapses, demonstrating unparalleled dual-modal plasticity and chemically-regulated neuromorphic functions through the interplay of internal photo-electric and external electrolyte-mediated chemical-electric processes. Electrical modulation by implementing closed or open-circuit enables switching of optoelectronic synaptic operation between short-term and long-term plasticity. Furthermore, inspired by transmembrane receptors that connect extracellular and intracellular events, synaptic responses can also be effectively amplified by applying chemical modifications to nanowire surfaces, which tune external and internal charge behaviors. Notably, under varied external electrolyte environments (ion/molecule species and concentrations), our device successfully mimics chemically-regulated synaptic activities and emulates intricate oxidative stress-induced biological phenomena. Essentially, we demonstrate that through the nanowire photoelectrochemical synapse configuration, optoelectronic synapses can be incorporated with chemical-electric behaviors to bridge the gap between classic optoelectronic synapses and biological synapses, providing a promising platform for multifunctional neuromorphic applications.

Bioinspired and biomimetic electronics, drawing inspiration from the functionalities and concepts of living systems, have significantly propelled the evolution of highly efficient and intelligent artificial systems[1–5]. Among these, optoelectronic synapses, which integrate the classic photo-electric effect with synaptic plasticity, have attracted extensive interest due to high computing speed, low crosstalk, expansive bandwidth, and superior energy efficiency[6,7]. Moreover, optoelectronic synapses can perceive, preprocess, and memorize

e-mail: haiding@ustc.edu.cn

visual information, laying the foundation for pioneering artificial visual systems[8,9], including motion detection[10], in-sensor computing[11], and neuromorphic bionic eyes[12]. Despite these exciting progresses, a disparity in operation principles still exists, rendering conventional semiconductor-based synapses somewhat less versatile than their biological counterparts. Typically, most optoelectronic synapses mainly rely on photo-electric processes and charge carrier trapping mechanisms in semiconductors[13,14], in which the behaviors of electrons and holes play key roles in synaptic functions. This is in sharp contrast with their real biological counterparts, which are controlled by a series of small molecule and ion-mediated processes, namely, electrolyte-mediated chemical-electric processes, such as neurotransmitter release, ion migration, and action potential transmission[15].

Consequently, such disparity in operation mechanisms could limit the potential of optoelectronic synapses for diverse tunability and multifunctional applications. For instance, semiconductor-based optoelectronic synapses often face biocompatibility challenges and lack chemical tunability. Conversely, biological synapses, functioning in complex chemical environments, exhibit remarkable responsiveness to their chemical surroundings[15], which endows living systems with multifaceted biological functionalities[16,17]. Therefore, it is imperative to bridge the significant gap between biological synapses, which involve electrolyte-mediated chemical-electric processes, and existing optoelectronic synapses, which mainly rely on photo-electric physical processes, in order to emulate advanced chemical-related neuromorphic functions and complex biological activities seldomly reported in previous optoelectronic synapses[7,18]. Most recently, photoelectrochemical devices, which are built upon semiconductor optoelectronic materials surrounded by an electrolyte environment, naturally operate in aqueous conditions for versatile photosensing and biosensing[19–22]. The device characteristics are governed by the interplay between internal semiconductor physical processes based on electron/hole dynamics and external electrolyte-mediated chemical reactions involving molecule and ion-associated activities[21], offering us a promising platform for constructing advanced optoelectronic synapses with biorealistic functionalities.

Herein, we report an optoelectronic synapse with rich chemical tunability based on the simple photoelectrochemical architecture composed of p-AlGaN/n-GaN semiconductor nanowires. Harnessing the interplay of internal photoexcited charge transport/accumulation and external electrolyte-mediated charge transfer/consumption, our device demonstrates unique synaptic features, notably dual-modal synaptic plasticity, along with extensive chemically-regulated neuromorphic functions. Remarkably, based on the distinct hole accumulation mechanisms, the device can flexibly switch between current mode, showing short-term plasticity, and voltage mode, exhibiting long-term plasticity, by simply changing the circuit states (either closed or open-circuit). In current mode, the device exhibits PPF index of 217% and synaptic behavior lasting for approximately 60 s, whereas in voltage mode, it shows PPF index of 293% and synaptic behavior lasting for over 1500 s. Furthermore, inspired by the transmembrane receptors in biological synapses, chemical modification (e.g., Pt nanoparticle decoration) was introduced to the semiconductor surface, which effectively modulated external charge consumption and internal charge transport, leading to amplified synaptic responses with the current response doubling and the voltage response slightly increasing. More impressively, by manipulating chemical-electric processes through varying ion species, concentrations, or introducing specific biochemical molecules, the external charge consumption behavior can be regulated, resulting in chemically-regulated synaptic activities and emulating complex oxidative stress-related biological phenomena including cognition and vision decline. This photoelectrochemical synaptic device, which combines internal physical and external electrolyte-mediated chemical processes, serves as a promising candidate for constructing advanced artificial systems connecting optoelectronic synapses with biological functionalities.

Results

Concept of the photoelectrochemical synapse

The human visual system plays a pivotal role in our interactions with the environment, accounting for more than 80% of our sensory input from the external world[8]. As depicted in Fig. 1a (top panel), light information is perceived by photoreceptors in retina, converted into neural signals, and subsequently transmitted via optic nerves to brain for image processing and memorization. The entire visual system, including the eyes, optic nerves, and brain, operates within biological environments (i.e., physiological electrolytes). Electrolyte-mediated chemical-electric processes, such as conducting action potentials and maintaining electrical neutrality, form the foundation for basic visual activities. In this context, its functionality is sensitive to changes in the electrolyte environment, as manifested by alcohol-induced visual function deterioration[23] and oxygen-free radical-induced visual loss[24,25]. Essentially, changes in the complex chemical environment directly affect the electrolyte-mediated activities in photoreceptors and synapses, subsequently altering visual behaviors and endowing living systems with diverse biological activities. Therefore, to emulate advanced chemically-regulated functions and devise biorealistic artificial visual systems, it is imperative to develop optoelectronic synaptic devices based on photo-electric behaviors while incorporating electrolyte-mediated chemical-electric processes.

To mimic the chemical-electric synaptic behaviors, we propose an artificial synaptic device based on a photoelectrochemical architecture using p-AlGaN/n-GaN nanowire arrays as a fundamental element for advanced artificial visual systems (more detailed discussion about the photoelectrochemical architecture is available in Supplementary Note 1). As concisely illustrated in Fig. 1a (bottom panel), our device works within aqueous environments and is inherently surrounded by various ions and molecules, which is the prerequisite for electrolyte-mediated activities exhibited in biological synapses. Upon illumination, charge carriers are generated in the nanowires. Some of the charge carriers accumulate within the nanowires, resulting in photo-electric synaptic responses. Concurrently, the ions and molecules in the electrolyte consume a portion of the charge carriers, which emulates the molecule and ion-associated behaviors in living systems (i.e., electrolyte-mediated chemical-electric processes), thus producing diverse chemical-related synaptic functions. By leveraging the internal physical and external electrolyte-mediated chemical processes, the synaptic activities of our device could be manipulated by physical or chemical approaches (Fig. 1b). Through applying closed or open-circuit state, the optoelectronic synaptic operation can switch between current mode and voltage mode, exhibiting short-term and long-term plasticity, respectively (Fig. 1b left; details are shown in Section 2). Additionally, the synaptic responses can be modulated by employing chemical modification on nanowire surface or varying the external electrolyte surroundings (Fig. 1b right; details are shown in Section 4 and 5). Such combined internal physical and external electrolyte-mediated chemical processes fundamentally differ from those in previously reported solid-state or electrolyte-gated synaptic devices, and thus give rise to distinctive neuromorphic characteristics and functionalities (mechanisms and functionalities of our device and other synaptic devices are summarized and compared in Supplementary Note 2). Furthermore, the aqueous electrolyte environment containing ions and molecules is crucial in the construction of the photoelectrochemical synapse. More details on the importance of ion use can be found in Supplementary Note 3.

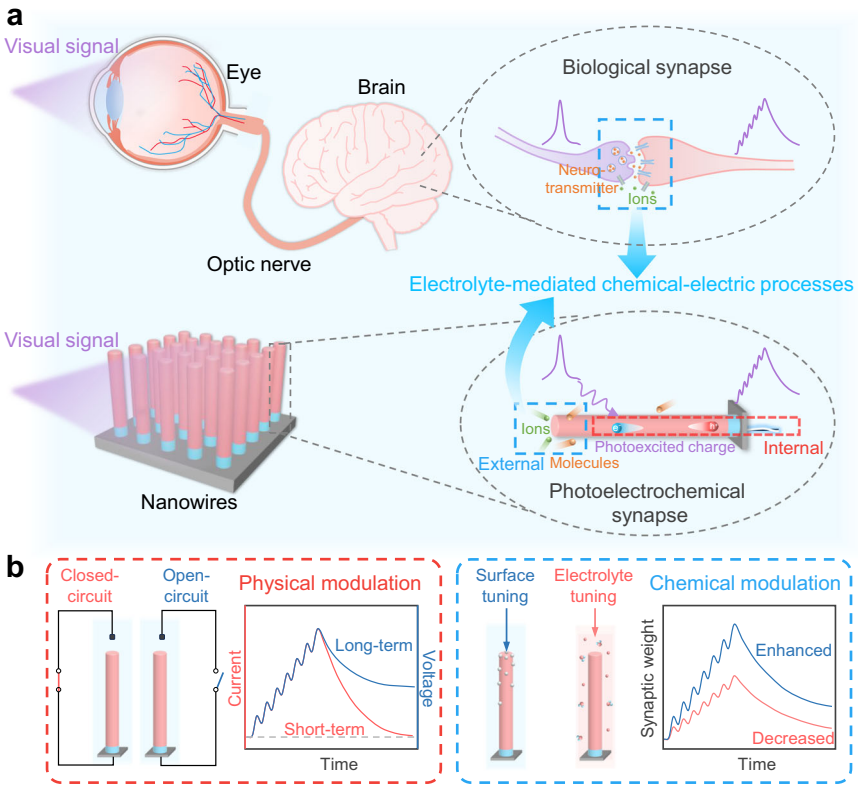

Fig. 1 | Schematics of the biological visual system and the photoelectrochemical synapse. a Schematic of biological visual system (top) and photoelectrochemical synapse (bottom). Both biological synapses and photoelectrochemical synapses operate through electrolyte-mediated chemical-electric processes in aqueous environments. Additionally, the photoelectrochemical synapses also rely on internal physical (photo-electric) processes involving hole/electron transfer behaviors. **b** Schematic of the synaptic activity modulation by physical (left) and chemical approaches (right) in the photoelectrochemical synapses. By manipulating the physical dynamics, the device can switch between current mode and voltage mode, showing short-term and long-term plasticity, respectively. Through the application of chemical methods, including surface chemical modification and varying the electrolyte environment, synaptic responses can be regulated.

Dual-modal optoelectronic synaptic behaviors through physical modulation

Gallium nitride (GaN) materials exhibit excellent optoelectronic and piezoelectric properties[21,26]. In recent years, there have been notable works utilizing GaN materials, including micro/nanowires and cantilever structures, for the development of strain-sensitive electrical synapses[26–30] and optoelectronic synapses[31,32]. GaN materials demonstrate good chemical stability in electrolyte solution, making it suitable for research involving electrolyte-mediated chemical reactions[33]. Furthermore, GaN materials exhibit tunable bandgap and show promising prospects for device integration[34]. During epitaxial growth, the bandgap of GaN materials can be controlled by adjusting the alloy composition (e.g., AlGaN or InGaN), enabling the material system to cover a broad spectrum from ultraviolet to near-infrared[34]. More importantly, GaN-based nanowires, characterized by high crystalline quality and large surface-to-volume ratio, are particularly attractive in optoelectronic applications due to their superior light absorption and charge carrier behaviors[33,35]. Additionally, in an aqueous environment, the large surface area of the one-dimensional structure makes the nanowires exceptionally sensitive to electrolyte solutions[36,37], ideal for constructing optoelectronic synapses with chemical-related functions. Thereby, in our study, p-AlGaN/n-GaN heterojunction nanowires grown on n-Si substrate via plasma-assisted molecular beam epitaxy (MBE) are exploited to build up the photoelectrochemical synaptic device (Fig. 2b). The scanning electron microscopy (SEM) images in Fig. 2c show that the as-grown nanowires are vertically aligned on the n-Si substrate. In these nanowires, p-AlGaN/n-GaN heterojunction is introduced to regulate the charge carrier behaviors through the internal p–n junction. The heterojunction structure was displayed by scanning transmission electron microscopy (STEM) shown in Fig.2d, consisting of a ~ 250 nm p-AlGaN top segment and a ~ 20 nm n-GaN bottom segment. Additionally, we conducted high-resolution transmission electron microscopy (TEM) characterization of the as-prepared nanowires (Supplementary Fig. 13), which reveals clear lattice fringes of the GaN materials, indicating the excellent crystallinity of the nanowires grown through MBE.

The construction of photoelectrochemical synapse device is illustrated in Fig. 2b, which is straightforward involving primarily the formation of ohmic contact on the n-Si substrate followed by insulating epoxy encapsulation to prevent current leakage (see "Methods" for more details). Then, the device is integrated into a complete circuit loop by connecting the nanowire electrode and Pt mesh electrode using measurement unit like an electrochemical workstation or source meter. Finally, the nanowire electrode and Pt electrode are immersed in an electrolyte solution to complete the device assembly.

To mimic biological synapses and further investigate artificial synaptic activities in biological environments, a physiological electrolyte, specifically phosphate buffered saline (PBS) solution at pH value of 7.4, was selected as the electrolyte in our photoelectrochemical synapse investigations, and an electrochemical workstation was used for recording the response. Under closed-circuit conditions, light stimuli act as presynaptic inputs to trigger postsynaptic current (ΔPSC) within the circuit (i.e., current mode). As shown in Fig. 2a(i), the device demonstrates typical excitatory synaptic response upon ten consecutive stimuli of 255 nm light with pulse duration (t_p) of 0.2 s and pulse interval (Δt) of 0.2 s. The ΔPSC gradually

https://doi.org/10.1038/s41467-024-51194-z

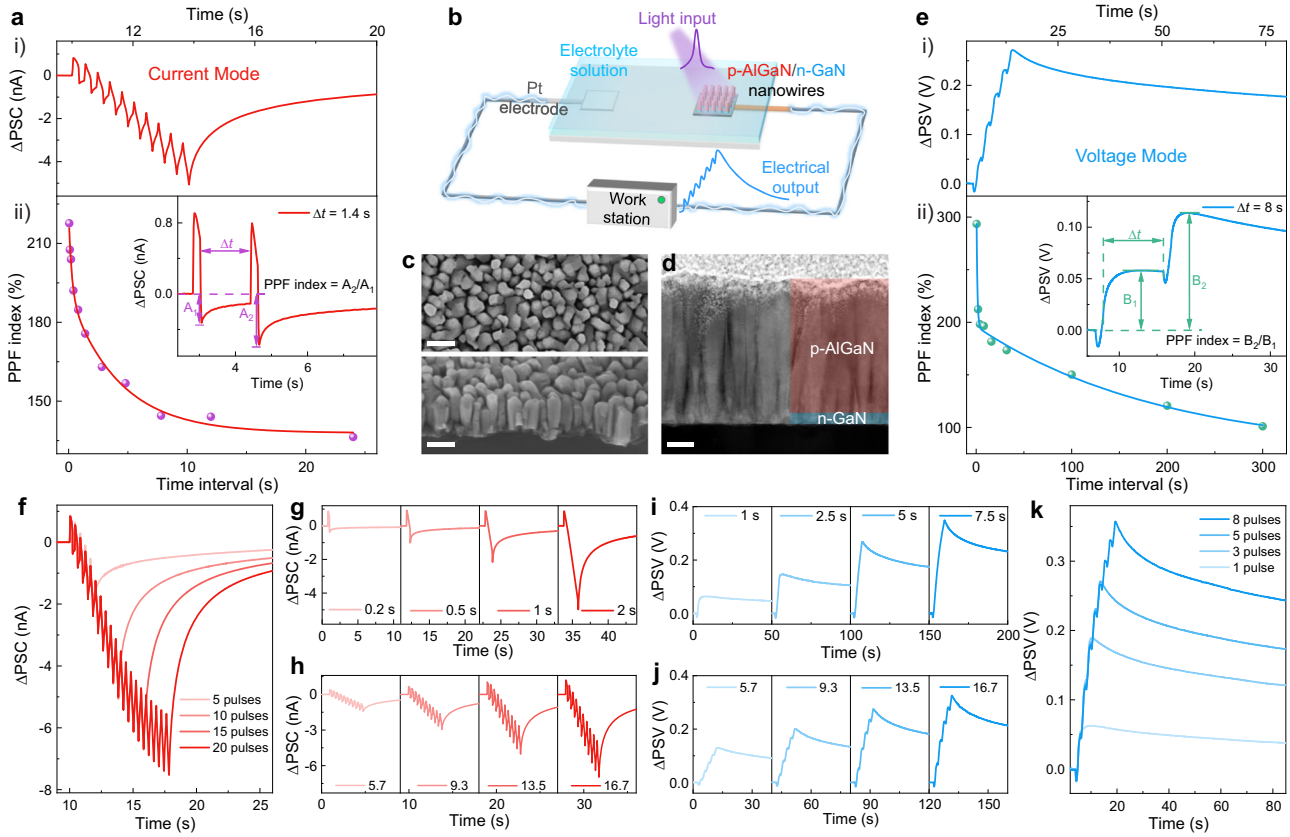

Fig. 2 | Structure and dual-modal synaptic behaviors of the photoelectrochemical synapse. a i): Postsynaptic current (ΔPSC) in response to ten light pulses ($t_p = \Delta t = 0.2$ s); ii): PPF index versus pulse interval, with the inset showing the PPF effect and its definition. **b** Schematic of the photoelectrochemical synaptic device. **c** Top-view SEM image (top; scale bar, 150 nm) and 45°-tilted SEM image of the as-grown nanowires (bottom; scale bar, 150 nm). **d** STEM image of the as-grown nanowires (scale bar, 50 nm). **e** i): Postsynaptic voltage (ΔPSV) induced by five light pulses ($t_p = \Delta t = 1$ s); ii): PPF index versus pulse interval, with the inset showing the PPF effect and its definition. **f**-**h** Correlations between ΔPSC and pulse number (**f**), pulse duration (**g**), and pulse intensity (**h**). **i**–**k** Correlations between ΔPSV and pulse number (**k**), pulse duration (**i**), and pulse intensity (**j**). Light pulses of 12 μW cm^{-2} were used, except for the pulse intensity-dependent tests. The inset numbers in (**h**) and (**j**) represent different light intensities from 5.7 to 16.7 μW cm^{-2}.

decays to the original state after stimulation and the synaptic response lasts for approximately 60 s (Supplementary Fig. 7), successfully emulating the short-term plasticity (STP) observed in biological synapses. Moreover, paired-pulse facilitation (PPF), a typical STP property, is achieved by applying two sequential light pulses to the device (inset of Fig. 2a(ii)). The PPF index is defined as $A_2/A_1 \times 100\%$, where A_1 and A_2 are the ΔPSC values following the first and second stimulus, respectively. As exhibited in Fig. 2a(ii), the device shows the maximum PPF index of 217% and the PPF index decreases as the time interval between the two pulses increases. The correlation between PPF index and time interval in our device can be well fitted with a double exponential decay function, consistent with the PPF characteristics of biological synapses[38].

Furthermore, biological synapses dynamically respond to varying external stimuli and modulate their synaptic strength accordingly[39]. To simulate the dynamic activities in response to different external stimuli, the optoelectronic synaptic responses of the photoelectrochemical synapse under different pulse numbers, durations, intensities, and frequencies were evaluated. Figure 2f shows the postsynaptic current of our device regulated by controlling pulse number. As the external stimuli increase from 5 to 20 pulses, the amplitude of ΔPSC increases accordingly. Similarly, the amplitude of ΔPSC gradually strengthens as the pulse duration, intensity, and frequency increase, as displayed in Figs. 2g, h, and Supplementary Fig. 15.

Impressively, beyond the common current mode, the photoelectrochemical synapse can also function under open-circuit conditions, leveraging light-regulated open-circuit voltage as the postsynaptic signal (ΔPSV) without changing the device structure or materials (i.e., voltage mode). Figure 2e(i) shows the typical synaptic response in voltage mode triggered by five consecutive 255 nm light pulses. The test with extended measurement time is depicted in Supplementary Fig. 14, with synaptic response lasting for over 1500 s in voltage mode. In contrast, while postsynaptic signals in current mode decay rapidly, ΔPSV undergoes a more gradual decay, demonstrating features of long-term plasticity (LTP). To illustrate the differences in the time-dependent trend of synaptic response in both modes, we normalize the postsynaptic current and voltage, as shown in Supplementary Fig. 7. After light pulses, the relaxation processes of the device in current mode and voltage mode are obviously different, with the postsynaptic current decaying rapidly while the postsynaptic voltage decays slowly. Thus, based on the circuit state (either closed-circuit or open-circuit), the photoelectrochemical synapse can operate in current mode (STP) or voltage mode (LTP), exhibiting dual-modal switchable synaptic behaviors. Additional synaptic functions, including PPF and pulse condition-dependent plasticity in voltage mode, were further investigated. As shown in the inset of Fig. 2e(ii), the amplitude of ΔPSV after the second pulse is greater than that after the first pulse, which is a clear indication of the PPF feature. The device shows the maximum PPF index of 293% and the PPF curve is well fitted using a double exponential decay function (Fig. 2e(ii)). Moreover, the amplitude of ΔPSV can be modulated by varying pulse parameters. With increasing pulse duration, intensity,

https://doi.org/10.1038/s41467-024-51194-z

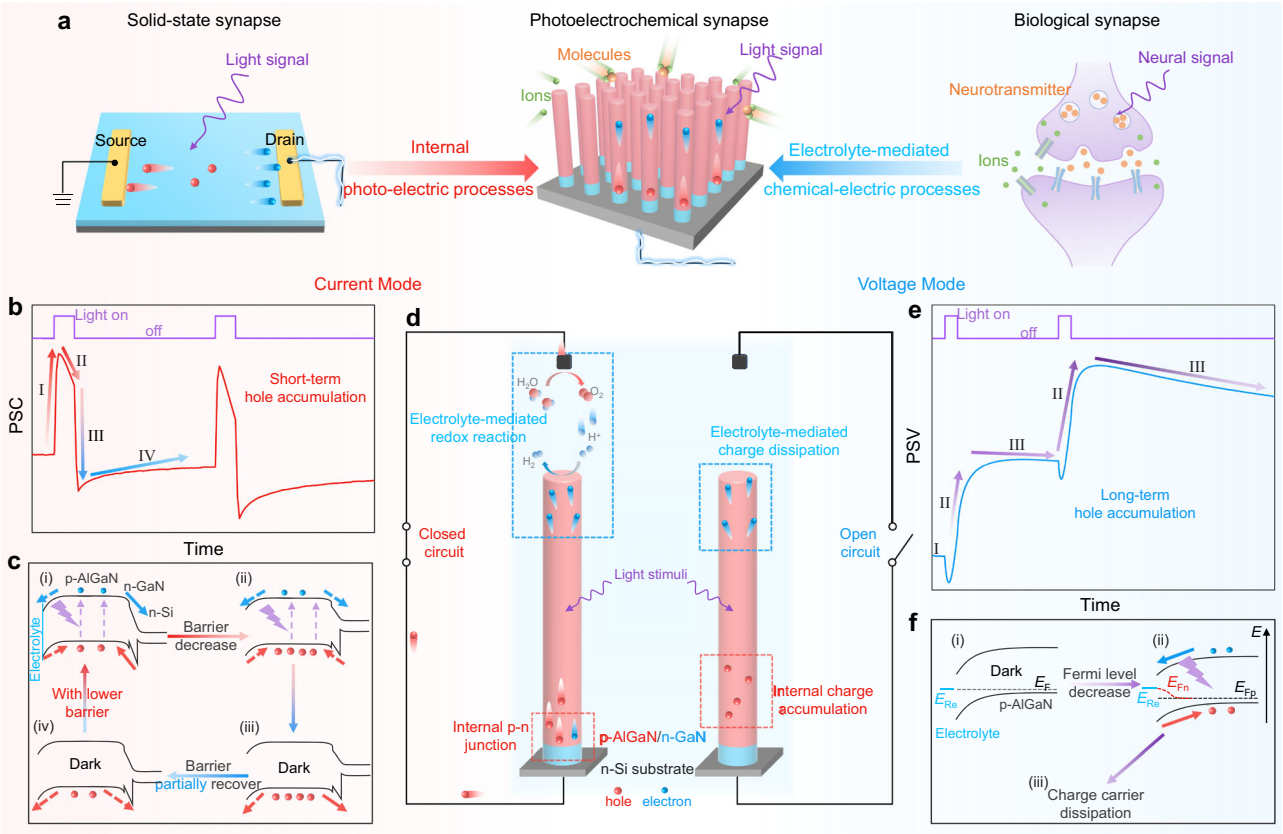

Fig. 3 | Working mechanisms of the photoelectrochemical synapse. **a** Comparison of our photoelectrochemical synapse with solid-state and biological synapses. **b** Representative postsynaptic current (PSC) triggered by two sequential pulses. **c** Schematic of band bending and charge carrier behaviors in current mode during the light stimulation (i & ii) and the dark recovery phase (iii & iv), illustrating short-term hole accumulation and barrier height modulation. Arrows are used to indicate the direction of charge carrier transport, with solid arrows representing the dominant charge carrier transfer direction. **d** Schematic of the charge carrier dynamics upon light stimulation in closed (left) and open (right) circuit, involving the internal nanowire and electrolyte-mediated charge behaviors. **e** Typical post-synaptic voltage (PSV) induced by two successive pulses. **f** Schematic of band bending and charge carrier behaviors in voltage mode during the initial dark state (i), the light stimulation (ii), and the post-stimulation recovery in the dark (iii).

and number, the ΔPSV amplitude increases accordingly (Figs. 2i–k). Clearly, such a unique voltage mode offers an alternative approach for realizing synaptic activities under open-circuit state. As displayed in Fig. 2, the photoelectrochemical synapse demonstrates current in the nA level in current mode. In future work, we aim to integrate micro/nanofabrication processes to further downscale the device dimensions, thereby lowering device current and power consumption. Interestingly, compared with the nA level current observed in current mode, devices operating in voltage mode exhibit no static current and can work without an electric power supply. Moreover, previous study reports that the device performance under open-circuit conditions is independent of its device size[40], indicating the possibility for device miniaturization. Consequently, the voltage mode operation of photoelectrochemical synapses not only provides an alternative way for synaptic behaviors but also presents potential avenues for advanced miniaturization and energy-efficient neuromorphic applications.

Overall, the proposed photoelectrochemical synaptic device exhibits a straightforward design that is not only easy to fabricate but also capable of operating within biocompatible environments. With the same structure and materials, the device can flexibly switch between open and closed-circuit mode, leading to different synaptic activities. Such switchable dual-modal characteristics enable tailored operational modes for specific needs, making it promising for constructing intricate neuromorphic systems.

Interplay of internal photo-electric and electrolyte-mediated chemical-electric processes

Following the investigation of the synaptic responses of the photoelectrochemical synapse, we propose that these synaptic activities are enabled by the interplay between internal photo-electric processes and external electrolyte-mediated chemical-electric processes, as schematically shown in Fig. 3a. Moreover, the dual-modal synaptic plasticity is based on the distinct charge storage dynamics within the nanowires. Before elucidating the operation mechanisms of the dual-modal behavior, we first briefly introduce the concept of semiconductor surface band bending in an electrolyte environment. When a p-type (n-type) semiconductor is immersed in an electrolyte environment, charge transfer occurs between the semiconductor and electrolyte, leading to downward (upward) band bending at the semiconductor/electrolyte interface[41]. Considering that the nanowire is predominantly composed of p-AlGaN, there is a downward surface band bending at the nanowire/electrolyte interface, which is in the opposite direction to the built-in electric field of internal p–n junction (Fig. 3c). We use arrows to depict the direction of the built-in electric fields, as shown in Supplementary Fig. 9, indicating that the directions of the two electric fields are opposite. Additionally, for clarity, the relationship between the direction of charge carrier movement and the polarity of current (voltage) in our device is schematically shown in Supplementary Fig. 9 and described as follows: In current mode, when electrons flow towards the electrolyte, the current is negative; when

electrons transfer towards the external circuit, the current is positive. In voltage mode, electron movement towards the electrolyte produces a positive voltage spike, while electron movement towards the Si substrate leads to a negative voltage spike. The electrical signal polarity definitions are summarized in Supplementary Note 7. The detailed discussions on the working mechanisms are as follows.

Under the closed-circuit, photoexcited electrons and holes are generated upon light stimuli, predominantly within the p-AlGaN segment (Fig. 3d, left). Given the opposite built-in electric fields of the nanowire/electrolyte junction and the internal p–n junction, electrons tend to flow towards both the electrolyte (undergoing chemical redox reactions with protons) and the external circuit (exhibiting positive current). When electrons are consumed by the aqueous electrolyte ($4e^- + 4H^+ \rightarrow 2H_2$), corresponding holes flow to Pt electrode and are consumed by the electrolyte ($4h^+ + 2H_2O \rightarrow O_2 + 4H^+$), due to the conduction and valence band edges of AlGaN straddle water redox potentials[33,42]. Additionally, we conducted gas chromatography analysis to verify the generation of H_2 and O_2 under extreme test conditions (i.e., high applied bias, long duration), as shown in Supplementary Fig. 11. Detailed discussion on interface redox reactions can be found in Supplementary Note 8. During the transport of electrons, due to the slower charge transfer and consumption at the electrolyte interface[43,44], the current flow towards the external circuit dominates (Fig. 3c(i)), resulting in a positive current spike in the postsynaptic current (PSC) curve (process I in Fig. 3b). Importantly, because of the opposite electric fields, holes might temporarily accumulate within the nanowires. As the holes gradually accumulate, the built-in electric field strength decreases (Fig. 3c(ii)), leading to fewer electrons flowing to the external circuit and consequently, a decreased positive current (process II in Fig. 3b). During the dark recovery phase, only the accumulated holes remain within the nanowires. These holes produce significant barrier height reduction, facilitating the flow of holes either towards the external circuit or being consumed by the electrolyte. Due to the sluggish hole-associated redox reactions at the electrolyte interface[43,45], namely, slow hole transfer and consumption at the electrolyte/semiconductor interface, holes primarily migrate to the external circuit (Fig. 3c(iii)), leading to a transient negative shift when the light is off (process III in Fig. 3b). As the accumulated holes gradually migrate and get consumed, the barrier returns to the original state, consistent with the PSC relaxation (process IV). In essence, the two opposite built-in electric fields result in hole storage within the nanowires, giving rise to history-dependent behaviors. Moreover, under closed-circuit conditions, the accumulated holes either flow towards the external circuit or migrate to the electrolyte, undergoing redox reactions, leading to short-term hole storage and exhibiting STP characteristics.

Under the open-circuit, as illustrated in Fig. 3d (right), considering the absence of current flowing through the circuit and that the photoexcited charge carriers remain within the nanowire electrode, we primarily focus on the nanowire/electrolyte interface. In addition, for better understanding, the relationship between the semiconductor Fermi level and the recorded open-circuit voltage can be summarized as follows: an increase in the semiconductor Fermi level corresponds to a negative shift of the recorded voltage, while a decrease corresponds to a positive shift of the voltage[46]. In the dark, as depicted in Fig. 3f(i), the Fermi level of the semiconductor (E_F) equilibrates with redox pairs in electrolyte (E_{re}), characterized as the open-circuit voltage (PSV). Upon illumination, E_F splits into quasi-Fermi levels of electrons (E_{Fn}) and holes (E_{Fp}). The downward surface band bending drives the electrons towards the electrolyte, which are compensated by positively charged species in the electrolyte[46], aligning E_{Fn} with E_{re} (Fig. 3f(ii)). In this context, the extent of surface band bending is reduced[46], and E_{Fp} decreases relative to the initial E_F, leading to a positive shift of PSV, consistent with process II in Fig. 3e. During the recovery phase, the stored holes gradually dissipate through reactions with substances in the electrolyte, leading to PSV decay (process III). It is noteworthy that the initial negative voltage peak in the PSV curve upon light stimulus corresponds to the positive current peak in the PSC curve, both attributed to the internal p–n junction induced electron movement towards the Si substrate[44]. Essentially, the photoexcited charge carriers remain within the semiconductor electrode under open-circuit conditions, and the surface band bending further results in the accumulation of majority charge carriers within the semiconductor, altering the PSV and exhibiting synaptic behaviors. Additionally, the photoexcited charge carriers cannot flow to the external circuit and can only be consumed by the electrolyte, giving rise to slow charge dissipation and LTP characteristics.

In summary, as illustrated in Fig. 3d, both modes involve photoexcited charge accumulation within the nanowires and electrolyte-mediated charge consumption. The internal photo-electric synaptic processes resemble those in conventional solid-state synapses, while the external electrolyte-mediated chemical-electric processes draw inspiration from their biological counterparts (Fig. 3a). The quantitative comparison of the photo-electric and chemical-electric processes can be found in Supplementary Note 5. Distinctively, the short-term hole accumulation in current mode is enabled by the opposite built-in electric fields at the semiconductor/electrolyte interface and the internal p–n junction. In contrast, the voltage mode is more straightforward, with the open-circuit condition offering the basis for long-term hole accumulation. The unique charge accumulation mechanisms lead to their distinct synaptic behaviors. To further validate the proposed mechanisms, we prepared additional nanowire samples, including p-GaN directly grown on n-Si substrate (p-GaN/n-Si) and n-GaN directly grown on n-Si substrate (n-GaN/n-Si). Based on above principles, the p-GaN/n-Si with an internal p–n junction would demonstrate both PSC and PSV responses, whereas the n-GaN/n-Si, lacking a p–n junction, is anticipated to only exhibit PSV response under open-circuit conditions. As shown in Supplementary Fig. 4, our experimental results are consistent with the predictions, confirming the feasibility of our proposed mechanism and indicating potential expandability into other material systems. The above experiments demonstrate the necessity of the p–n junction for achieving synaptic responses in current mode. To further illustrate the necessity of the electrolyte/semiconductor junction, we fabricated solid-state devices using p-AlGaN/n-GaN nanowires and tested the photoresponse, as shown in Supplementary Fig. 5. The solid-state device exhibits typical photodetector behaviors due to the p–n junction. In the photoelectrochemical synapse, the electrolyte environment creates a downward surface band bending at the p-AlGaN/electrolyte interface, thereby introducing two opposite built-in electric fields for carrier storage and synaptic behavior. Furthermore, to illustrate the necessity of controlling the length of p-n nanowire, we prepared additional p–n junction nanowires by maintaining the length of the p-AlGaN while increasing the length of the n-GaN to 200 nm. The test results are shown in Supplementary Fig. 6. It is observed that compared to nanowires with a 20 nm n-GaN segment, increasing the length of n-GaN substantially enhances the positive current peak in current mode. Correspondingly, in voltage mode, this leads to significantly large negative voltage peaks, resulting in unclear curve shapes and difficulty in discerning synaptic behavior. Therefore, in our device, besides introducing p–n junction to achieve carrier storage, we also need to rationally control the length of the p- and n- segment in the p–n junction to control synaptic behaviors.

Bridging the internal and external processes: chemical modification on the semiconductor surface

As previously discussed, the photoelectrochemical synapse functions via the interplay between internal photo-electric and external electrolyte-mediated chemical-electric processes. On the one hand, similar to previous semiconductor-based synapses, charge

https://doi.org/10.1038/s41467-024-51194-z

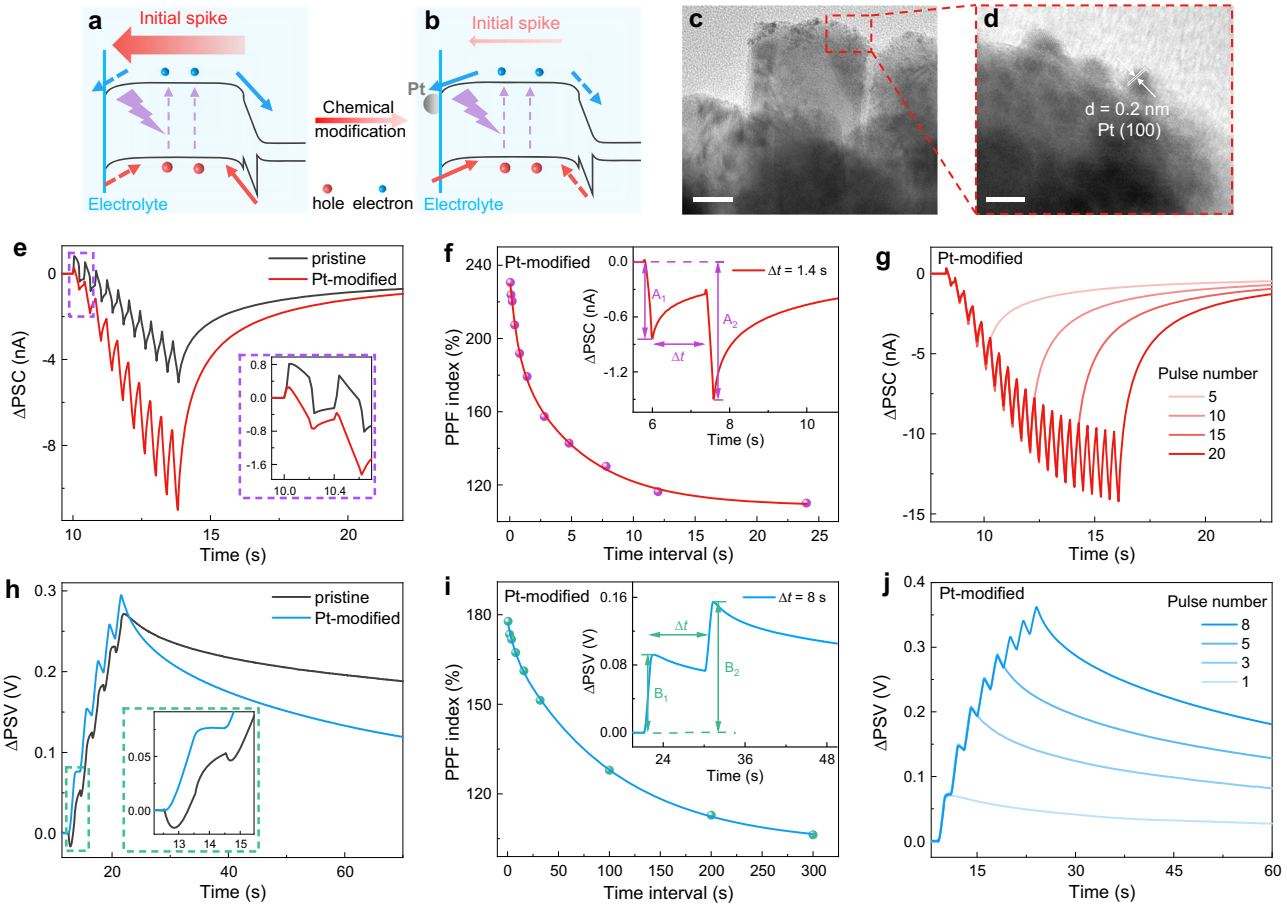

Fig. 4 | Synaptic plasticity modulation via surface Pt modification. **a**, **b** Schematic illustrations of the charge carrier behaviors before (**a**) and after (**b**) anchoring Pt nanoparticles on the nanowire surface. Arrows are used to indicate the direction of charge carrier transport, with solid arrows representing the dominant charge carrier transfer direction. **c** TEM image of Pt-modified nanowires (scale bar, 25 nm). **d** HRTEM image of the red-outlined area (scale bar, 5 nm). **e**, **h** PSC curves (**e**) and PSV curves (**h**) of pristine device and Pt-modified device with the inset exhibiting an enlarged view of the synaptic responses. **f**, **i** PPF curves in current mode (**f**) and voltage mode (**i**) with Pt modification, with the inset showing the PPF effect. **g**, **j** Synaptic responses with different pulse numbers in current mode (**g**) and voltage mode (**j**). Light pulses of 255 nm and 12 μW cm^{-2} were used. In current mode, $t_p = \Delta t = 0.2$ s. In voltage mode, $t_p = \Delta t = 1$ s.

accumulation within the semiconductor leads to dual-modal synaptic responses. More importantly, the electrolyte-mediated charge consumption, which emulates the electrolyte-mediated processes in living systems, could incorporate biorealistic chemical tunability to our device. In biology, transmembrane receptors interact with specific ligands outside the cell. Upon ligand binding, these receptors initiate a series of intracellular events that modulate synaptic behaviors[47,48]. Inspired by the role of transmembrane receptors in bridging extracellular and intracellular events and regulating synaptic activity, we introduced chemical modification to the nanowire surface. These chemical modifications act as artificial receptors, which modulate the external electrolyte-mediated charge consumption and internal charge transport behaviors, thus tuning synaptic responses.

As a demonstration, in our photoelectrochemical synapse, chemical modification of anchoring platinum (Pt) nanoparticles on the nanowire surface is proposed. As discussed in Fig. 3, a pronounced positive current spike in the PSC curve can be observed for the pristine device upon illumination, which is attributed to the sluggish charge consumption via electrolyte-mediated processes and the movement of electrons to the external circuit. The corresponding charge carrier behaviors are schematically shown in Fig. 4a. It is widely acknowledged that Pt is one of the most efficient co-catalysts for chemical redox reactions, especially for reduction reactions, which could facilitate electron transfer to the electrolyte and electron consumption by the electrolyte[21,35]. After incorporating Pt modification, the chemical reactions at the nanowire/electrolyte interface could be facilitated, driving the internal electrons predominantly toward the electrolyte. As such, diminished positive current spike together with enhanced negative current could be realized (Fig. 4b).

Afterward, we modified the nanowires with Pt nanoparticles through photodeposition (details of the photodeposition process are provided in Methods). As shown in Figs. 4c and d, transmission electron microscopy (TEM) and high-resolution transmission electron microscopy (HRTEM) images confirm the successful introduction of Pt nanoparticles onto the nanowire surface, exhibiting the typical interplanar spacing of Pt (100) plane[44]. We then investigated the synaptic behaviors of this Pt-modified device. Compared with the pristine device, in current mode, the positive current spike in the Pt-modified device substantially decreases, while the negative current is significantly boosted, reaching twice that of the pristine device (Fig. 4e). This phenomenon is attributed to the optimized surface chemical reactivity with Pt modification, in agreement with the discussion in Fig. 4b. Similarly, in voltage mode, the negative voltage spike is considerably diminished. As discussed earlier, the voltage spike upon illumination arises from electron migration to the Si substrate through the internal p–n junction. The large reduction of the voltage spike indicates that the electron flow is dominant toward the electrolyte, in accordance with the discussion in Fig. 4b. Notably, a small positive PSC peak can be observed at the initial stage (inset of Fig. 4e), which is attributed to the fact that, even though Pt nanoparticle decoration

accelerates the interface chemical reactions, the chemical reactions and carrier consumption at the interface are still slower than the carrier drift within the semiconductor and circuit[43]. This inevitably leads to a small number of electrons flowing to the external circuit, manifested as the observed small positive PSC spike (detailed discussion is provided in Supplementary Note 5). Additionally, the observed rapid decay of ΔPSV with Pt decoration could be attributed to the promoted charge transfer with electrolyte by co-catalyst modification[49], leading to accelerated hole dissipation. Collectively, these experimental results indicate that introducing Pt modification into the photoelectrochemical synapse successfully accelerates charge consumption at the semiconductor/electrolyte interface and regulates internal charge movement, thus effectively tuning synaptic behaviors, consistent with our predictions. Moreover, the above discussions on the effects of Pt modification are based on the mechanism proposed in Fig. 3, and the experimental results agree well with our predictions, suggesting the reliability of our mechanisms.

Other synaptic functions of the Pt-modified device were also studied, including PPF and pulse condition-dependent plasticity. As exhibited in Figs. 4f and i, the Pt-modified device exhibits typical PPF behaviors, which are fitted well with the dual exponential decay function. Moreover, the amplitudes of both ΔPSC and ΔPSV can be modulated by altering pulse conditions. With increasing number, intensity, and duration of optical pulses, the amplitude increases accordingly (Figs. 4g, j, and Supplementary Fig. 16). The cycle-to-cycle and device-to-device variations of the Pt-decorated synaptic device are summarized in Supplementary Fig. 8. In current mode, we compared the peak values after 10 pulses, while in voltage mode, we compared the peak values after 5 pulses. The variation is defined as the ratio of the standard deviation to the mean. For cycle-to-cycle variation, we tested 30 cycles. In voltage mode, the variation is 1.54%, whereas it is 3.08% in current mode. Regarding device-to-device variation, we prepared 10 devices. In voltage mode, the variation is 3.29%, and it is 3.04% in current mode. Clearly, the above results indicate that such chemical modification of Pt nanoparticles, acting as artificial receptors, effectively modulates synaptic behaviors without dismissing the synaptic activities. This finding suggests the potential for further implementation of other chemical modification strategies reported in previous photoelectrochemical devices, such as anchoring biomolecules (enzymes, antibodies, nucleic acids, and so on)[50] or forming encapsulation layers[36], to regulate synaptic activities and introduce biochemical functions into neuromorphic devices.

Electrolyte-mediated modulation of synaptic behaviors and oxidative stress effect simulation

In addition to surface chemical modification, the inherent electrolyte environment, which consists of various ions and molecules, naturally offers opportunities to modulate electrolyte-mediated charge dynamics and generate intriguing synaptic features similar to those observed in biological systems. In biology, synapses operate within a similar chemical environment where ions and molecules establish the foundation for synaptic activities. Changes in the chemical environment give rise to diverse synaptic and neural behaviors[51], further resulting in changes in biological activities. By exploiting the natural electrolyte-based working environment, such chemical regulation effects on synaptic activity and sophisticated biological activities can be emulated in the photoelectrochemical synapse by modulating the electrolyte-mediated charge consumption processes.

Here, we employed the Pt-modified device to investigate the electrolyte regulation effect. The ΔPSC responses to different concentrations of electrolyte were first examined. As shown in Fig. 5a (top), with increasing H_2SO_4 concentration, enhanced postsynaptic current was observed. Interestingly, upon the replacement of protons (H^+) with Na^+ ions (using Na_2SO_4 solution as the electrolyte), the synaptic device exhibited a diminished response with increasing Na_2SO_4 concentration (Fig. 5a, bottom). The regulation mechanism of H_2SO_4 solution is primarily attributed to change in proton concentration: the chemical reaction on p-AlGaN nanowires mainly involves the reduction reaction between protons and electrons ($2e^- + 2H^+ \rightarrow H_2$), in which the proton concentration significantly affects the reaction rate. As the proton concentration increases, the chemical reaction between electrons and protons accelerates, leading to the boosted negative current response[36,52]. Thus, increasing the H_2SO_4 concentration significantly enhances the synaptic response. When water is replaced with Na_2SO_4 solution, the concentration of conductive ions (i.e., the conductivity of the electrolyte) increases, leading to an increased consumption rate of both electrons and holes at the semiconductor/electrolyte interface. In this context, fewer holes flow to the circuit, resulting in a reduced negative current, manifested as the diminished postsynaptic current, consistent with previous report[36]. Further increasing the Na_2SO_4 concentration has little effect, which may be explained by considering that the increased conductivity of the electrolyte solution no longer significantly impacts synaptic performance, indicating that the influence of electrolyte conductivity has reached saturation. Additionally, the pH-dependent synaptic response was explored, as shown in Fig. 5b. As the pH value decreases, the postsynaptic current is noticeably enhanced due to the increased proton concentration. A more detailed discussion of the mechanisms of the chemical regulation effect is provided in Supplementary Note 8.

Moreover, we unitized bioactive molecules to regulate the synaptic response of the photoelectrochemical device within the physiological electrolyte (PBS solution). As illustrated in Fig. 5c, a significant reduction of ΔPSC response was observed upon the introduction of ascorbic acid (AA) into the PBS solution. With further increasing AA concentration, the response consistently diminished, exhibiting the modulation of synaptic activities by bioactive molecules. The molecule regulation effect arises from the electron donor role of AA, which can undergo oxidation reactions with holes ($AA + h^+ \rightarrow$ dehydro-ascorbic acid). This hole consumption reaction can easily happen and is more favorable than the default hole consumption reaction in aqueous electrolyte[53,54]. AA can capture holes and considerably facilitates hole consumption at the semiconductor/electrolyte interface. As a result, the holes flowing to the external circuit decrease, leading to a decrease in postsynaptic current. In conclusion, by manipulating ion type, ion concentration, and specific biochemical molecules in the electrolyte environment, we can effectively control the consumption rate of electrons and holes at the semiconductor/electrolyte interface, thereby modulating synaptic behaviors. In addition to chemical regulation effect, temperature also affects learning and memory behaviors in biological systems. In the photoelectrochemical synapse, the synaptic responses in PBS solution at different temperatures were investigated, as shown in Supplementary Fig. 17. As the electrolyte temperature increases, the ΔPSC response significantly increases. This behavior can be attributed to the temperature sensitivity of both the photo-electric and chemical-electric processes, with higher temperature accelerating chemical reactions at the electrolyte/semiconductor interface and giving rise to larger current[55]. Moreover, a temperature increase within a certain range can enhance the photoresponse of photodetectors[56].

To further demonstrate the potential of our device for simulating intricate biological activities, we emulated the age-related cognitive decline caused by oxidative stress (i.e., the free-radical theory of aging)[24]. During the aging process, advancing age is positively correlated with both biological and cognitive degeneration[57]. Particularly, oxidative stress[57,58], an outcome of the imbalance between reactive oxygen species (ROS) and antioxidants, leads to synaptic dysfunction and cellular damage, playing a pivotal role in the development of age-related diseases, as conceptually depicted in Fig. 5d. Additionally, the cognitive impairment induced by oxidative stress is illustrated in

https://doi.org/10.1038/s41467-024-51194-z

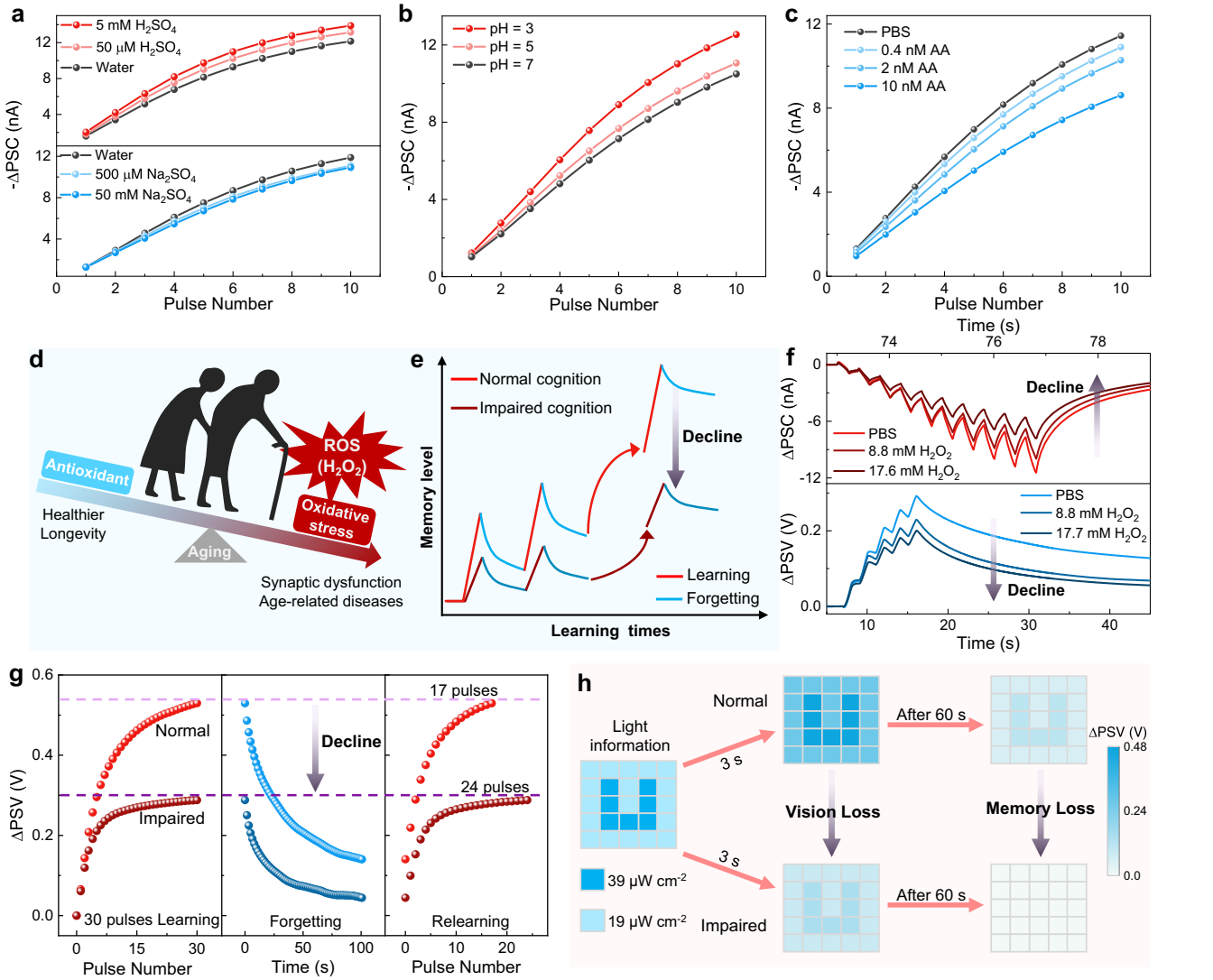

Fig. 5 | Electrolyte-regulated synaptic plasticity and simulation of oxidative stress-associated biological activities. a ΔPSC responses to various concentrations of H_2SO_4 solution (top) and Na_2SO_4 solution (bottom). **b** ΔPSC responses in 0.1 M Na_2SO_4 solution at different pH values. **c** ΔPSC responses in PBS solution with various concentrations of ascorbic acid (AA). **d** Schematic illustration of the balance between reactive oxygen species (ROS) and antioxidants in humans. Excessive ROS leads to synaptic dysfunction and age-related diseases. **e** Schematic illustration of cognitive decline caused by excessive ROS. **f** Synaptic responses in PBS solution with different concentrations of H_2O_2. **g** Learning-forgetting-relearning behavior under normal and impaired conditions simulated by the photoelectrochemical synapse. **h** The simulation of visual perception and memory under normal and impaired conditions using the photoelectrochemical synapse. Light pulses of 255 nm and 12 μW cm^{-2} were used. In current mode, $t_p = \Delta t = 0.2$ s. In voltage mode, $t_p = \Delta t = 1$ s. Note that we take the absolute value of the postsynaptic current (-ΔPSC) for performance comparison in Figs. 5a, b, and c.

Fig. 5e. Human learning inherently progresses from initial knowledge acquisition to long-term retention in a step-by-step manner. While newly acquired knowledge tends to fade over time, repetitive learning leads to better remembering and retention. Nevertheless, under an oxidative stress state, excessive ROS production, like hydroxyl radical (•OH) and hydrogen peroxide (H_2O_2)[58], results in cellular damage and synaptic dysfunction, which subsequently triggers learning and memory capability decline (the darker curve).

Then, H_2O_2 was introduced into the PBS solution to mimic oxidative stress-associated biological activities. Upon the addition of H_2O_2, both the postsynaptic current and voltage were obviously attenuated (Fig. 5f), similar to the biological synaptic degeneration induced by the overproduction of ROS. The diminished synaptic responses are due to the hole scavenger role of H_2O_2 ($H_2O_2 + 2\,h^+ \rightarrow O_2 + 2H^+$), which can easily happen and is more favorable than the default hole consumption reaction in aqueous electrolyte[59]. H_2O_2 can capture holes and facilitate hole consumption at the electrolyte/semiconductor interface and reduces the holes flowing to the external circuit, resulting in weakened synaptic behaviors. It is noteworthy that although protons are generated when H_2O_2 is consumed, the electrolyte used is PBS buffer solution, and the pH remains essentially unchanged. More detailed discussion of the H_2O_2 regulation effect is provided in Supplementary Note 8. Additionally, the cognitive decline shown in Fig. 5e is emulated in our device in voltage mode, as exhibited in Fig. 5g. First, 30 consecutive light pulses were applied to the device as the learning process. The impaired device (with 17.7 mM H_2O_2 addition) exhibited a lower learning level. After the stimulus removal of 100 s, the impaired device displayed reduced memory retention. More importantly, during the relearning process, the normal device (without H_2O_2) required only 17 pulses to recover to the initial learning level, whereas the impaired device required 24 pulses, suggesting pronounced degeneration in learning and memory capabilities. Apart

from cognitive decline, excessive ROS also leads to retinal cell injury and vision loss[25], which is also demonstrated in our optoelectronic synaptic device. During the simulation, a "U" image was constructed by utilizing stimuli of different light intensities, as demonstrated in Fig. 5h. Following a light stimulus of 3 s, the normal device manifested a distinct "U" image, whereas the impaired device displayed obvious vision loss with diminished contrast and brightness in the image. After the forgetting process of 60 s, the "U" image in the impaired device became indiscernible, whereas the normal one still exhibited superior memory retention. It is noteworthy that all data were obtained from the same device. Conclusively, the above results demonstrate that the photoelectrochemical synapse not only mimics the temperature and chemical modulation effect similar to biological synapses but also emulates complicated oxidative stress-associated biological phenomena including cognition and vision decline. These findings not only offer insights for the advancement of artificial systems capable of simulating authentic biological activities but also highlight the potential for direct interfacing with biological systems by virtue of the inherent electrolyte-based working environment and electrolyte-mediated processes. Additional discussions on the biocompatibility of the device and its relevance to biological systems can be found in Supplementary Note 3.

Discussion

In conclusion, we present a dual-modal photoelectrochemical synaptic device with rich chemical-related neuromorphic functions based on the interplay between its internal charge carrier dynamics and external electrolyte-mediated charge consumption behaviors. Through distinct hole storage within the nanowires, the device demonstrates switchable synaptic plasticity between current mode (STP) and voltage mode (LTP). Furthermore, by incorporating chemical modification of Pt nanoparticles, the electrolyte-mediated charge consumption behaviors are promoted, and internal charge transport is regulated, leading to amplified synaptic responses. More interestingly, by manipulating the temperature and chemical surroundings of the electrolyte environment (changing ion type, concentration or introducing specific biochemical molecules), our synaptic device displays temperature-dependent synaptic responses and chemically-regulated synaptic activities similar to biological synapses, and successfully emulates complicated oxidative stress-associated biological activities based on the human aging theory.

In the photoelectrochemical synapse, while the dual-modal feature offers switchable operational modes and synaptic behaviors, it also requires further research to meet the demands of multifunctional applications. In our future work, we aim to leverage the CMOS-compatible and low-cost silicon platform, along with micro/nano-fabrication techniques, to develop large-scale photoelectrochemical synaptic device arrays. Furthermore, by developing peripheral readout circuits, the simultaneous application of PSC and PSV functions on a single chip can be realized. Despite these challenges, we anticipate that this novel photoelectrochemical synaptic device, distinguished by its intriguing device characteristics and simple structure, could not only serve as a promising building block for multisensory artificial systems that integrate visual and chemical clues but also provide great possibilities for combined optoelectronic and biochemical neuromorphic applications, such as photoelectrochemical neuromorphic biosensing and optical brain-machine interface.

Methods

Growth of p-AlGaN/n-GaN semiconductor nanowires

The p-AlGaN/n-GaN heterojunction nanowires were grown on an n-type Si (111) substrate under nitrogen-rich conditions using plasma-assisted MBE. The Si substrate was first cleaned with acetone and methanol to remove organic contaminants, followed by a hydrofluoric acid wash to remove native oxides. Subsequently, the cleaned Si substrate was loaded into the MBE chamber. Before initiation of the growth, the substrate was annealed to ensure the removal of the residual oxides. Nitrogen radicals were delivered from a radio frequency plasma source. Fluxes of Al, Ga, Mg, and Si were controlled using thermal effusion cells. The p-AlGaN and n-GaN segment was grown at 780 °C by doping with Mg and Si, respectively.

Material characterization

The SEM images were obtained using field-emission scanning electron microscope (Hitachi SU8220) operated at 3 kV. STEM image was captured using FEI Talos F200X instrument operated at 200 kV. TEM and HRTEM images were acquired using JEM-2100PLUS instrument operated at 200 kV.

Photodeposition process of Pt nanoparticles

Pt nanoparticles were anchored onto the surface of the nanowires through photodeposition method at room temperature. Before photodeposition, the nanowire sample was cleaned with acetone, isopropanol, and water to remove organic contaminants. Subsequently, the sample was immersed in a solution containing 8 ml deionized water, 2 ml methanol, and 15 μl H_2PtCl_6 solution (20 mg ml^{-1}). The precursor solution was then illuminated with Hg lamp for 15 minutes. After the photodeposition process, the nanowire sample was rinsed with deionized water at least three times and finally dried with N_2 gas.

Nanowire photoelectrode fabrication

The fabrication process for the nanowire photoelectrode is as follows: The native oxide layer on Si substrate was first removed, and then Ga-In eutectic (Alfa Aesar) was painted on the substrate to establish ohmic contact. Subsequently, the nanowire sample was mounted to copper sheet using silver paste (SPI Supplies). Afterward, insulating epoxy was used to encapsulate the photoelectrode except the nanowires to prevent current leakage. Finally, the photoelectrode was dried in air at room temperature. After drying for 24 h, the nanowire photoelectrode was used for optoelectronic experiments. For the solid-state device, Ni/Au and Ti/Au are employed for ohmic contacts, serving as the p-side and n-side contacts, respectively.

Optoelectronic synaptic activity measurements

During the assessment of synaptic responses, a three-electrode configuration was utilized. The nanowire photoelectrode, Pt counter electrode, and saturated Ag/AgCl reference electrode were placed inside a high-ultraviolet-transmittance quartz cell. 1x PBS solution (Sangon Biotech) was used as the electrolyte solution unless stated otherwise. All tests were conducted at room temperature (25 °C), unless stated otherwise. An electrochemical workstation (CHI 660E) was employed to record the current and voltage signals. In the three-electrode configuration, the nanowire electrode and Pt counter electrode formed the current loop. The reference electrode served as the voltage reference, and the applied bias was set between the nanowire photoelectrode and the reference electrode. Detail discussion about the three-electrode configuration can be found in Supplementary Note 1. Figure 2b shows a simplified illustration of the device structure without reference electrode, while a comprehensive layout of the three-electrode configuration is presented in Supplementary Fig. 2. In current mode, an applied bias of 0 V was maintained. The light stimulus was provided by a LED with wavelength of 255 nm, and the light intensity was calibrated using an optical power meter (Newport Model No. 2936 R). The light pulse frequency was controlled through arbitrary waveform generator (Rigol DG1022U). Under extreme testing conditions, an H-shaped cell was used for investigation (details are shown in Supplementary Note 8). The collected gases after regular and extreme tests are analyzed by gas chromatography (Agilent 8860 gas chromatograph).

Data availability

The data that support the findings of this study are available in the article, supplementary information file, source data file or from the corresponding authors upon request. Source data are provided in this paper.

References

1. Yang, X. et al. Bioinspired neuron-like electronics. *Nat. Mater.* **18**, 510–517 (2019).
2. Jiang, L. et al. Flexible ultrasound-induced retinal stimulating piezo-arrays for biomimetic visual prostheses. *Nat. Commun.* **13**, 3853 (2022).
3. Ling, Y. et al. Bioinspired elastomer composites with programmed mechanical and electrical anisotropies. *Nat. Commun.* **13**, 524 (2022).
4. Kim, Y. et al. A bioinspired flexible organic artificial afferent nerve. *Science* **360**, 998–1003 (2018).
5. Liao, F. et al. Bioinspired in-sensor visual adaptation for accurate perception. *Nat. Electron.* **5**, 84–91 (2022).
6. Sun, Y., Ding, Y. & Xie, D. Mixed-dimensional Van Der Waals heterostructures enabled optoelectronic synaptic devices for neuromorphic applications. *Adv. Funct. Mater.* **31**, 2105625 (2021).
7. Hao, D., Yang, Z., Huang, J. & Shan, F. Recent developments of optoelectronic synaptic devices based on metal halide perovskites. *Adv. Funct. Mater.* **33**, 2211467 (2023).
8. Li, G. et al. Photo-induced non-volatile VO(2) phase transition for neuromorphic ultraviolet sensors. *Nat. Commun.* **13**, 1729 (2022).
9. Chen, K. et al. Organic optoelectronic synapse based on photon-modulated electrochemical doping. *Nat. Photon.* **17**, 629–637 (2023).
10. Chen, J. et al. Optoelectronic graded neurons for bioinspired in-sensor motion perception. *Nat. Nanotechnol.* **18**, 882–888 (2023).
11. Wu, X. et al. Wearable in-sensor reservoir computing using optoelectronic polymers with through-space charge-transport characteristics for multi-task learning. *Nat. Commun.* **14**, 468 (2023).
12. Long, Z. et al. A neuromorphic bionic eye with filter-free color vision using hemispherical perovskite nanowire array retina. *Nat. Commun.* **14**, 1972 (2023).
13. Farronato, M. et al. Reservoir computing with charge-trap memory based on a MoS(2) channel for neuromorphic engineering. *Adv. Mater.* **35**, 2205381 (2023).
14. Yu, J. R. et al. Bioinspired mechano-photonic artificial synapse based on graphene/MoS2 heterostructure. *Sci. Adv.* **7**, eabd9117 (2021).
15. Thoenen, H. Neurotrophins and neuronal plasticity. *Science* **270**, 593–598 (1995).
16. Woods, B. J. & Van Vactor, D. miRNA: local guardians of presynaptic function in plasticity and disease. *RNA Biol.* **18**, 1014–1024 (2021).
17. Bara, A., Ferland, J.-M. N., Rompala, G., Szutorisz, H. & Hurd, Y. L. Cannabis and synaptic reprogramming of the developing brain. *Nat. Rev. Neurosci.* **22**, 423–438 (2021).
18. Wang, X., Zong, Y., Liu, D., Yang, J. & Wei, Z. Advanced optoelectronic devices for neuromorphic analog based on low-dimensional semiconductors. *Adv. Funct. Mater.* **33**, 2213894 (2023).
19. Fang, S. et al. Light-induced bipolar photoresponse with amplified photocurrents in electrolyte-assisted bipolar p–n junction. *Adv. Mater.* **35**, 2300911 (2023).
20. Chen, W. et al. Manipulating surface band bending of iii-nitride nanowires with ambipolar charge-transfer characteristics: a pathway toward advanced photoswitching logic gates and encrypted optical communication. *Adv. Mater.* **36**, 2307779 (2024).
21. Wang, D. et al. Bidirectional photocurrent in p–n heterojunction nanowires. *Nat. Electron.* **4**, 645–652 (2021).
22. Wang, C. et al. Ultrafine silver nanoparticle encapsulated porous molecular traps for discriminative photoelectrochemical detection of mustard gas simulants by synergistic size-exclusion and site-specific recognition. *Adv. Mater.* **34**, 2202287 (2022).
23. Martino, F. et al. Deterioration of binocular vision after alcohol intake influences driving performance. *Sci. Rep.* **11**, 8904 (2021).
24. Guo, J. et al. Aging and aging-related diseases: from molecular mechanisms to interventions and treatments. *Signal Transduct. Target. Ther.* **7**, 391 (2022).
25. Calderon, G. D., Juarez, O. H., Hernandez, G. E., Punzo, S. M. & De la Cruz, Z. D. Oxidative stress and diabetic retinopathy: development and treatment. *Eye* **31**, 1122–1130 (2017).
26. Zhang, S. et al. Strain-controlled power devices as inspired by human reflex. *Nat. Commun.* **11**, 326 (2020).
27. Hua, Q. et al. Piezotronic synapse based on a single GaN microwire for artificial sensory systems. *Nano Lett.* **20**, 3761–3768 (2020).
28. Zhou, X. et al. Magnetosensory power devices based on algan/gan heterojunctions for interactive electronics. *Adv. Electron. Mater.* **9**, 2200941 (2023).
29. Hua, Q. et al. Flexible GaN microwire-based piezotronic sensory memory device. *Nano Energy* **78**, 105312 (2020).
30. Liu, H. et al. A bamboo-like GaN microwire-based piezotronic memristor. *Adv. Funct. Mater.* **26**, 5307–5314 (2016).
31. Hong, X. et al. Two-dimensional perovskite-gated AlGaN/GaN high-electron-mobility-transistor for neuromorphic vision sensor. *Adv. Sci.* **9**, 2202019 (2022).
32. Chang, K.-C. et al. Optoelectronic dual-synapse based on wafer-level GaN-on-Si device incorporating embedded SiO2 barrier layers. *Nano Energy* **125**, 109564 (2024).
33. Zhou, P. et al. Solar-to-hydrogen efficiency of more than 9% in photocatalytic water splitting. *Nature* **613**, 66–70 (2023).
34. Kuykendall, T., Ulrich, P., Aloni, S. & Yang, P. Complete composition tunability of InGaN nanowires using a combinatorial approach. *Nat. Mater.* **6**, 951–956 (2007).
35. Wang, D. et al. Pt/AlGaN nanoarchitecture: toward high responsivity, self-powered ultraviolet-sensitive photodetection. *Nano Lett.* **21**, 120–129 (2021).
36. Wang, D. et al. Observation of polarity-switchable photoconductivity in III-nitride/MoSx core-shell nanowires. *Light.: Sci. Appl.* **11**, 227 (2022).
37. Kang, Y. et al. Achieving record-high photoelectrochemical photoresponse characteristics by employing Co(3)O(4) nanoclusters as hole charging layer for underwater optical communication. *ACS Nano* **17**, 3901–3912 (2023).
38. Zucker, R. S. & Regehr, W. G. Short-term synaptic plasticity. *Annu. Rev. Physiol.* **64**, 355–405 (2002).
39. Sun, Y. et al. Photoelectric synaptic plasticity realized by 2D perovskite. *Adv. Funct. Mater.* **29**, 1902538 (2019).
40. Dong, B., Zhang, X., Jiang, X. & Wang, F. Size-independent reconfigurable logic gate with bismuth oxide based photoelectrochemical device. *J. Am. Chem. Soc.* **145**, 4969–4974 (2023).
41. Kibria, M. G. et al. Visible light-driven efficient overall water splitting using p-type metal-nitride nanowire arrays. *Nat. Commun.* **6**, 6797 (2015).
42. Biswas, M., Chavan, V., Zhao, S., Mi, Z. & Chakrabarti, S. Passivation of surface states of AlGaN nanowires using H3PO4 treatment to enhance the performance of UV-LEDs and photoanodes. *ACS Appl. Nano Mater.* **1**, 1968–1975 (2018).
43. Yang, W. et al. Time-resolved observations of photo-generated charge-carrier dynamics in Sb2Se3 photocathodes for photoelectrochemical water splitting. *ACS Nano* **12**, 11088–11097 (2018).
44. Fang, S. et al. Tuning the charge transfer dynamics of the nanostructured GaN photoelectrodes for efficient photoelectrochemical detection in the ultraviolet band. *Adv. Funct. Mater.* **31**, 2103007 (2021).
45. Wan, J. et al. Exploring the polarization photocatalysis of ZnIn2S4 material toward hydrogen evolution by integrating cascade electric

fields with hole transfer vehicle. *Adv. Funct. Mater.* **32**, 2203252 (2022).
46. Zhang, Y., Guo, W., Zhang, Y. & Wei, W. D. Plasmonic photoelectrochemistry: in view of hot carriers. *Adv. Mater.* **33**, 2006654 (2021).
47. Ross, R. S. The extracellular connections: the role of integrins in myocardial remodeling. *J. Card. Fail.* **8**, S326–S331 (2002).
48. Jose, J., Ghantasala, S. & Roy Choudhury, S. Arabidopsis transmembrane receptor-like kinases (RLKs): a bridge between extracellular signal and intracellular regulatory machinery. *Int. J. Mol. Sci.* **21**, 4000 (2020).
49. Li, H.-M. et al. Synergetic integration of passivation layer and oxygen vacancy on hematite nanoarrays for boosted photoelectrochemical water oxidation. *Appl. Catal., B* **284**, 119760 (2021).
50. Shu, J. & Tang, D. Recent advances in photoelectrochemical sensing: from engineered photoactive materials to sensing devices and detection modes. *Anal. Chem.* **92**, 363–377 (2020).
51. Xiong, T. et al. Neuromorphic functions with a polyelectrolyte-confined fluidic memristor. *Science* **379**, 156–161 (2023).
52. Fang, J. et al. Photobase effect for just-in-time delivery in photocatalytic hydrogen generation. *Nat. Commun.* **11**, 5179 (2020).
53. Saha, S., Yang, J., Masouleh, S. S. M., Botton, G. A. & Soleymani, L. Hot hole direct photoelectrochemistry of Au NPs: interband versus intraband hot carriers. *Electrochim. Acta* **404**, 139746 (2022).
54. Xu, X. et al. Ascorbic acid as an effective antioxidant additive to enhance the efficiency and stability of Pb/Sn-based binary perovskite solar cells. *Nano Energy* **34**, 392–398 (2017).
55. He, B. et al. General and robust photothermal-heating-enabled high-efficiency photoelectrochemical water splitting. *Adv. Mater.* **33**, 2004406 (2021).
56. Yang, L. et al. Temperature-dependent photodetection behavior of AlGaN/GaN-based ultraviolet phototransistors. *Appl. Phys. Lett.* **120**, 091103 (2022).
57. Tan, B. L., Norhaizan, M. E., Liew, W.-P.-P. & Sulaiman Rahman, H. Antioxidant and oxidative stress: a mutual interplay in age-related diseases. *Front. Pharmacol.* **9**, 1162 (2018).
58. Finkel, T. & Holbrook, N. J. Oxidants, oxidative stress and the biology of ageing. *Nature* **408**, 239–247 (2000).
59. Chu, S. et al. Solar water oxidation by an InGaN nanowire photoanode with a bandgap of 1.7 eV. *ACS Energy Lett.* **3**, 307–314 (2018).

Acknowledgements

This work was funded by the National Natural Science Foundation of China (Grant no. 62322410, 52272168, 52161145404), the Fundamental Research Funds for the Central Universities (Grant no. WK3500000009), and International Projects of the Chinese Academy of Sciences (CAS) under Grant no. 211134KYSB20210011. The work was partially carried out at the USTC Center for Micro and Nanoscale Research and Fabrication. Additionally, this work was partially carried out at the Instruments Center for Physical Science, University of Science and Technology of China.

Author contributions

X.L., D.W., and W.C. contributed equally to this work. H.S. conceived the idea and designed the experiments. H.S., S.L., B.S.O., and L.F. discussed the experiment details. X.L., D.W., W.C., Y.K., and S.F. performed the sample preparation and characterizations. X.L., D.W., Y.L., D.L., H.Y., H.Z., and K.L. carried out the optoelectronic performance measurements and collected and analyzed the experimental data. X.L., D.W., and H.S. wrote the manuscript. All authors discussed the results and participated in the final version of this manuscript.

Competing interests

The authors declare no competing interests.

Additional information

Supplementary information The online version contains supplementary material available at https://doi.org/10.1038/s41467-024-51194-z.

Correspondence and requests for materials should be addressed to Haiding Sun.

Peer review information *Nature Communications* thanks Guozhen Shen, and the other, anonymous, reviewer(s) for their contribution to the peer review of this work. A peer review file is available.

Reprints and permissions information is available at http://www.nature.com/reprints

Publisher's note Springer Nature remains neutral with regard to jurisdictional claims in published maps and institutional affiliations.

Xin Liu[1,5], Danhao Wang[1,5], Wei Chen[1,5], Yang Kang[1], Shi Fang[1], Yuanmin Luo[1], Dongyang Luo[1], Huabin Yu[1], Haochen Zhang[1], Kun Liang[1], Lan Fu[2], Boon S. Ooi[3], Sheng Liu[4] & Haiding Sun[1]

[1]iGaN Laboratory, School of Microelectronics, University of Science and Technology of China, Hefei, Anhui, China. [2]Department of Electronic Materials Engineering, Research School of Physics and Engineering, The Australian National University, Canberra, ACT, Australia. [3]Computer, Electrical, and Mathematical Sciences and Engineering Division, King Abdullah University of Science and Technology, Thuwal, Saudi Arabia. [4]The Institute of Technological Sciences, Wuhan University, Wuhan, Hubei, China. [5]These authors contributed equally: Xin Liu, Danhao Wang, Wei Chen. e-mail: haiding@ustc.edu.cn